Synthesis of a Sinter-Resistant, Mixed-Oxide Support for Au Nanoclusters†

B. K. Min, W. T. Wallace, and D. W. Goodman*

Department of Chemistry, Texas A&M University, P.O. Box 30012, College Station, Texas 77842-3012

Received: February 16, 2004

Following the discovery that small gold clusters highly dispersed on metal oxide supports are active catalysts at low temperature for a variety of reactions, a number of studies have been carried out to determine the structure of the clusters and the mechanism leading to their activity. A major deterrent to the use of these catalysts, however, is that under reaction temperatures and pressures, the clusters tend to sinter, or agglomerate, leading to a dramatic decrease in activity. In an attempt to make these highly active Au catalysts more stable, mixed-oxide supports have been developed by substituting Ti atoms for Si in a silica thin film network. Depending on the amount of Ti deposited, the TiO_2-SiO_2 surface consists of substituted Ti atoms and/or TiO_x islands. With deposition of Au onto these TiO_2-SiO_2 surfaces (at low and high Ti coverages), the substituted Ti and/or TiO_x islands act as Au cluster nucleation sites, leading to a marked increase in the cluster number density compared to the Ti-free SiO_2 surface. Furthermore, upon exposure of Au clusters nucleated on surfaces with TiO_x islands to reaction temperatures and pressures, the clusters do not sinter. These results demonstrate that it is possible to produce a supported Au catalyst where metal agglomeration is significantly inhibited, allowing the unique properties of Au nanoclusters to be fully exploited.

Introduction

Whereas bulk Au is inert, Au nanoclusters supported on metal oxide supports have unique catalytic properties and exhibit extraordinarily high activity for a number of reactions, including the low-temperature oxidation of carbon monoxide (CO).[1,2] More recently, it was discovered that Au nanoclusters supported on TiO_2 catalytically promote the epoxidation of propylene with extraordinarily high selectivity.[3−5]

Au nanoclusters have received considerable attention experimentally and theoretically where issues that underpin their unique catalytic properties have been addressed.[6−10] To date, these studies have concluded that the unusual catalytic properties are related to (1) a quantum size effect with respect to the thickness of the Au islands,[2] (2) defects on the metal oxide surface, such as oxygen vacancies,[6,7] and (3) the structure of the interface between the Au clusters and the metal oxide surface resulting from the strength of the metal−support interaction[8] and the preparation method.[9] Therefore, intrinsic effects related to the Au clusters and to the metal oxide support must be considered in order to fully optimize nanostructured Au catalysts. The most important factor in the interaction between Au clusters and metal oxide supports are the defects on the metal oxide support, since defects are a key to the nucleation and growth of metal clusters.[6,7] Control of the defect concentration and type could possibly lead to manipulation of the density and the size of the supported metal nanoclusters and to optimization of the metal−support interaction.

Another important factor for an efficient Au catalyst is stability of the Au clusters under reaction conditions. Au nanocluster catalysts are known to deactivate with reaction time. For example, the catalytic activity of a typical Au nanocatalyst for CO oxidation is greatly attenuated within 2 h[10] due to sintering of the Au clusters where the cluster size increases and the cluster density decreases.[11,12]

The TiO_2-SiO_2 system has attracted considerable attention in recent years due to the extensive use of this mixed oxide as a catalyst and its use as a support for photocatalysts, acid catalysts, and oxidation catalysts.[13] Moreover, Au nanoclusters supported on this mixed-oxide surface show activity for propylene epoxidation comparable to TiO_2-supported Au catalysts but with enhanced stability.[14,15] However, no systematic study of the properties of this mixed oxide has been undertaken. In this study, we prepared a TiO_2-SiO_2 thin film on a Mo(112) substrate and showed that Ti defects in the SiO_2 surface can control the density of Au nanoclusters. In addition, we showed that, as a support, this TiO_2-SiO_2 surface exhibits sinter-resistant properties for Au nanoclusters with respect to heating and exposure to elevated pressures of CO and O_2.

Experimental Section

All experiments were carried out in an ultrahigh vacuum (UHV) apparatus with a base pressure of 5×10^{-10} Torr, consisting of an elevated pressure reactor and a surface analytical chamber, the details of which are described elsewhere.[16] Briefly, the techniques available include X-ray photoelectron spectroscopy (XPS), Auger electron spectroscopy (AES), low-energy electron diffraction (LEED), and scanning tunneling microscopy (STM). Following preparation and characterization in the surface analytical chamber, the sample was transferred in situ into the elevated-pressure reactor whose pressure was measured by a MKS Baratron pressure gauge. Ultrahigh purity (99.999%) oxygen from MG industries and a Mo(112) crystal, oriented to $<0.25°$ (from Matek, Germany), were used in this study. The Mo(112) surface was cleaned by oxygen treatment and high-temperature annealing (2000 K), and the cleanliness was verified with AES. A thermocouple (W-5%Re/W-26%Re) was used to measure the surface temperature and to calibrate an optical

† Part of the special issue "Gerhard Ertl Festschrift".

* To whom correspondence should be addressed. E-mail: goodman@mail.chem.tamu.edu.

10.1021/jp0492974 CCC: $27.50 © 2004 American Chemical Society
Published on Web 05/12/2004

pyrometer (OMEGA OS3700). In the STM measurements, the optical pyrometer was used to measure the temperature.

Results and Discussion

Several reports detailing the preparation, characterization, and properties of SiO_2 thin films and subsequently deposited metal clusters have been published recently.[17−19] Ordered SiO_2 thin films[19] have been synthesized on a $p(2 \times 3)$-O reconstructed Mo(112) surface[20] via deposition of Si at room temperature followed by oxidation at 800 K in 1×10^{-7} Torr O_2 for 5 min and a subsequent anneal at 1150 K in 1×10^{-7} Torr oxygen for 30 min. The thickness was estimated to be 0.35 ± 0.05 nm based on the attenuation of the Mo AES signal and using an inelastic electron mean free path of 0.95 nm at 187 eV.[21] This film shows a very sharp $c(2 \times 2)$ LEED pattern (Figure 1a), implying long-range order, and a bulk band gap as measured by ultraviolet photoelectron spectroscopy (UPS) and metastable impact electron spectroscopy (MIES).[22] In addition, a very flat terrace structure (Figure 1b) with ~0.1 nm r.m.s. roughness is observed with STM. Atomically resolved STM shows a $c(2 \times 2)$ atomic array, consistent with the LEED pattern.[17,23]

The detailed structure of SiO_2 grown on a Mo(112) substrate is still in question. Freund and co-workers[17] proposed a silica structure in which each silicon atom is tetrahedrally coordinated to four oxygen atoms bridging between two adjacent silicon atoms. These authors also suggested a Frank−van der Merwe growth mode for multilayer SiO_2 thin films. Studies in our laboratories indicate that a highly ordered, epitaxial film can be achieved only for a single layer. In this monolayer film, the silicon atoms are assumed to bind to the Mo substrate via oxygen atoms, forming a Mo−silicate structure within the interfacial region. Depending on the number of oxygen atoms that bind to the Mo substrate at the interface, three silicate structures are possible: nesosilicate (SiO_4^{4-}), inosilicate (SiO_3^{2-}), and phyllosilicate ($Si_2O_5^{2-}$).[25] On the basis of our STM data, the most probable structure is inosilicate in which two of the SiO_2 oxygen atoms are tetrahedrally bonded to the Mo substrate, with the remaining two oxygen atoms bridging the neighboring silicon atoms to form a chain-like structure.

XPS measurements were carried out for a clean SiO_2 thin film. Figure 1c shows O1s XPS data collected for a monolayer SiO_2 film. It is apparent that there are two different oxygen species with binding energies of approximately 530.3 and 532.0 eV. For comparison, O1s XPS spectra of oxygen-induced $p(2 \times 3)$ reconstructed Mo(112) and a thicker amorphous SiO_2 (2.7 ML) film were also investigated (data not shown). The binding energy for an oxygen-covered Mo(112) surface is 530.0 eV, similar to that measured for most alkaline-earth and transition-metal oxides such as MoO, MoO_2, CaO, and TiO_2.[26] On the other hand, covalent oxides such as SiO_2 have higher binding energies compared to the more ionic metal oxides. The reported values for the (O1s) binding energy of SiO_2 vary between 532.4 and 533.5 eV.[26] The thicker amorphous SiO_2 film shows only one feature at 532.2 eV, assigned to a Si−O−Si species. Recently, Black and co-workers published O1s XPS data for a crystalline calcium−silicate−hydrate surface as a function of the Ca/Si ratio.[27] With an increase in the Ca/Si ratio, the O1s spectra shows two features at 530.8 and 532.4 eV, assigned to oxygen of a Si−O−Ca species and oxygen of a Si−O−Si species, respectively. On the basis of these studies, the two features at 530.3 and 532.0 eV in the XPS spectrum of Figure 1c are assigned to Si−O−Mo and Si−O−Si, respectively.

In the chain structure proposed above, all 3-fold sites of the Mo substrate are occupied by oxygen atoms. However, due to repulsion between the oxygen atoms, every other oxygen moves toward the bridging sites of the Mo substrate, yielding the observed $c(2 \times 2)$ structure. In this structure there is a consequent height difference between the oxygen atom residing near the 3-fold site and the bridge-bonding oxygen atom. As a result, the silicon atoms are offset alternately to the left and right of the second Mo layer, forming a $c(2 \times 2)$ array. The higher-lying oxygen atoms bridging the silicon atoms are positioned between the second-row Mo atoms. This SiO_2 tetrahedral structure consists of continuous Si−O tetrahedra that share two oxygen atoms and contain Si−O−Mo and Si−O−Si species, giving rise to the two features observed in the XPS O1s spectra.

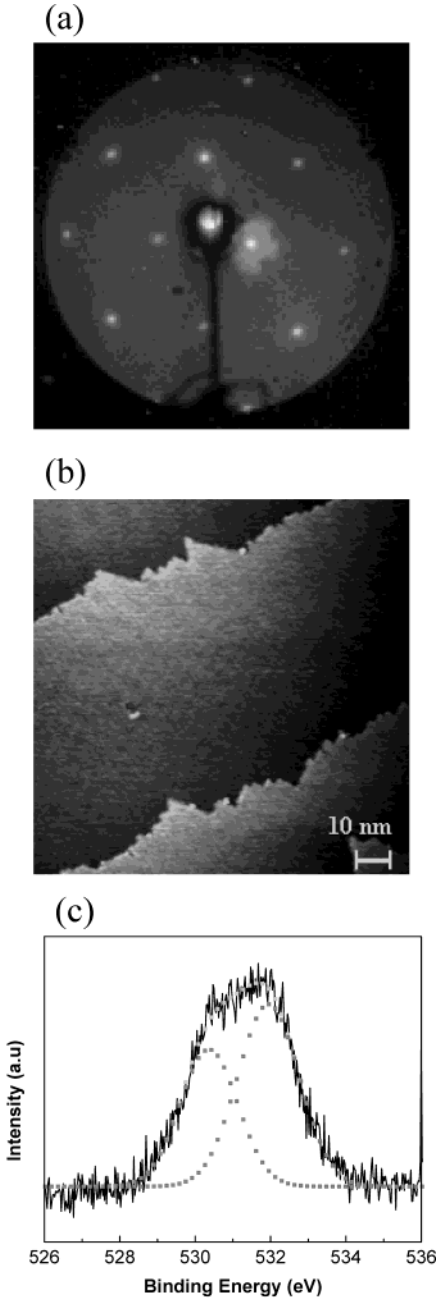

Figure 1. (a) LEED ($E = 56$ eV) and (b) STM image (100 nm × 100 nm) of a clean SiO_2 thin film ($U_s = -1.7$ V and $I = 0.18$ nA); (c) O1s XPS spectrum of a crystalline SiO_2 thin film (1.0 ML). The SiO_2 thin film was synthesized by deposition of Si on a $p(2 \times 3)$-O reconstructed Mo(112) surface followed by oxidation at 800 K and an anneal at 1150 K in oxygen.

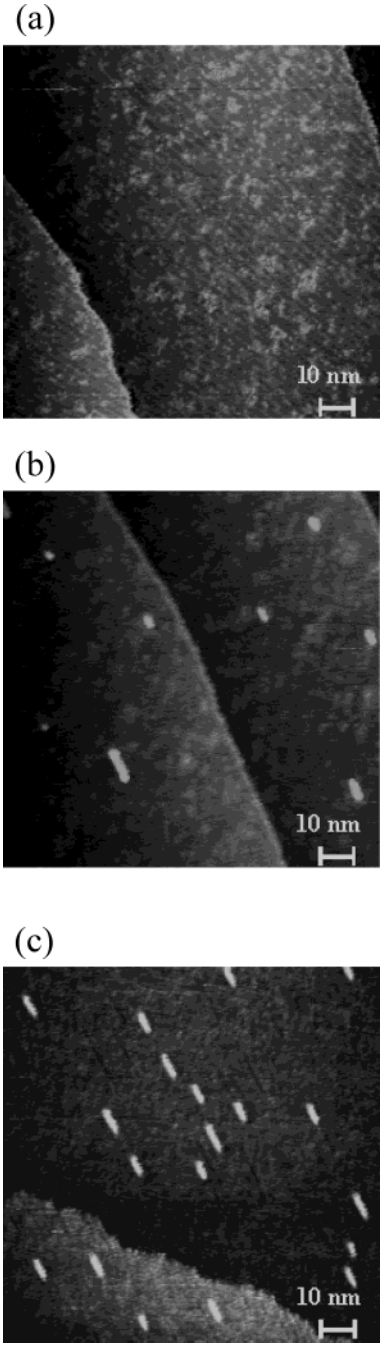

Figure 2. STM images (100 nm × 100 nm) of (a) a TiO_x-SiO_2 thin film with 8% Ti content ($U_s = -1.0$ V and $I = 0.18$ nA), (b) a TiO_x-SiO_2 thin film with 11% Ti content ($U_s = 1.0$ V and $I = 0.18$ nA), and (c) a TiO_x-SiO_2 thin film with 17% Ti content ($U_s = 1.0$ V and $I = 0.18$ nA). The titania−silica thin film was synthesized by deposition of Ti onto an SiO_2 surface followed by oxidation at 950 K and an anneal at 1150 K in a vacuum. Increasing Ti coverages lead to the formation of TiO_x islands on the surface.

Mixed oxides of silica and titania are known to form Si−O−Ti linkages and exhibit special properties with respect to photocatalysis and acid catalysis.[13] The structure of these mixed oxides is dependent on both the preparation method and chemical composition. It is generally believed that single phases of TiO_2-SiO_2 can only be obtained at low TiO_2 content, specifically at TiO_2 concentrations <15 wt %. At higher Ti concentrations, crystalline TiO_2 forms as a separate phase.[13] These general preparative guidelines were used in the synthesis of mixed-oxide films of SiO_2 and TiO_2.

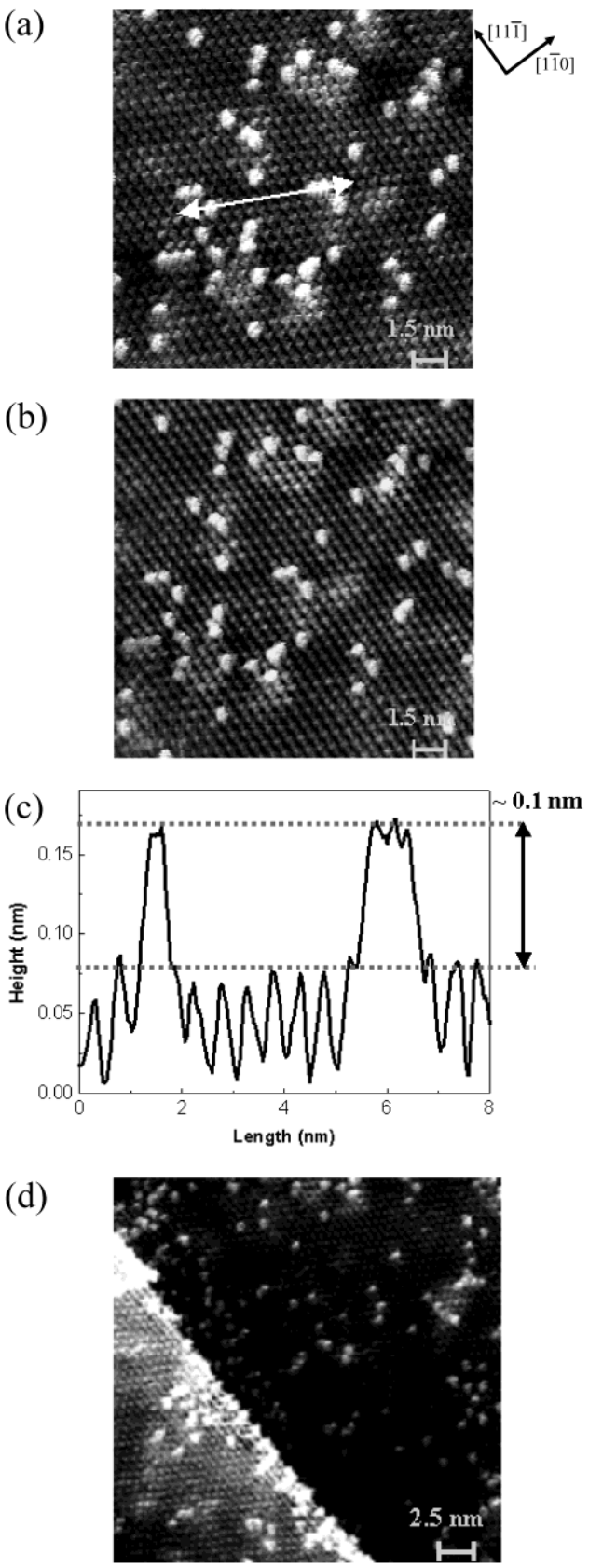

Figure 3. High-resolution STM images of a TiO_x-SiO_2 thin film with 8% Ti content: (a) local area of terrace (15 nm × 15 nm, $U_s = -1.0$ V, and $I = 0.18$ nA); (b) the same area as part (a) with reverse voltage bias (15 nm × 15 nm, $U_s = 1.0$ V, and $I = 0.18$ nA). The areas of bright contrast indicate atomically substituted Ti in the silica lattice. (c) Line profile along the arrow in part (a) showing the height difference between spots in bare SiO_2 and in brightest contrasts. (d) Local area of step edge (25 nm × 25 nm, $U_s = 1.0$ V, and $I = 0.18$ nA).

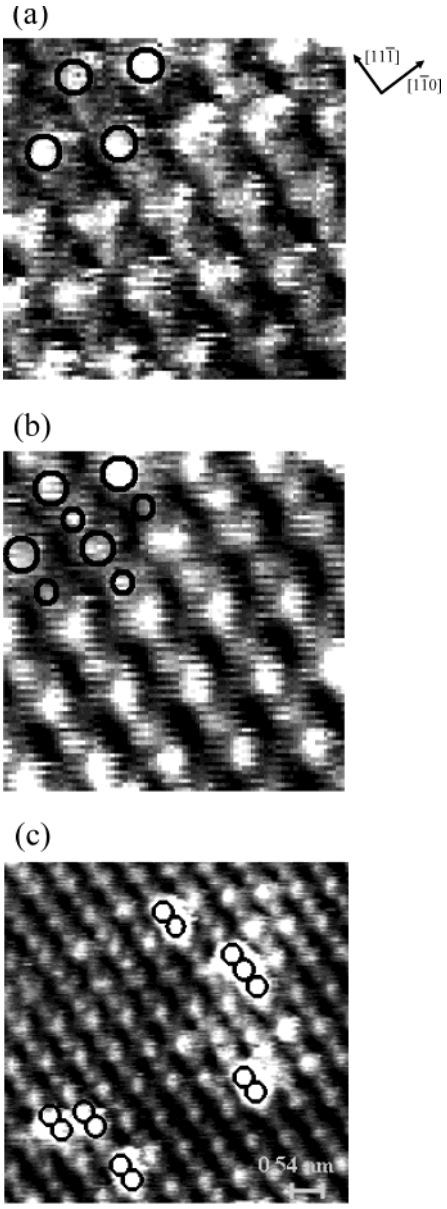

Figure 4. STM images of local areas of $TiO_2(8\%)-SiO_2$ thin film: (a and b) enlarged STM images (2.4 nm × 2.4 nm, $U_s = -1.0$ and 1.0 V, respectively) of the bare SiO_2 surface where open circles indicate a $c(2 \times 2)$ atomic array; (c) atomic resolution STM image (5.4 nm × 5.4 nm) where black open circles correspond to atomic corrugation of the bare SiO_2 surface showing that the brightest contrast spots correspond to the size of two atoms in the SiO_2 thin film.

A TiO_x-SiO_2 surface was prepared by deposition of Ti onto a SiO_2 thin film at room temperature, followed by oxidation at 950 K, and then an anneal in a vacuum at 1150 K. With deposition of Ti onto the SiO_2 film at room temperature, small, dense Ti clusters appear at the terraces and step edges. Oxidation at 950 K and an anneal to 1150 K leads to dramatic morphological changes in the TiO_x-SiO_2 surface. Parts a, b, and c of Figure 2 show Ti coverages of 8%, 11%, and 17%, respectively. The 8% Ti surface (Figure 2a) is very flat and essentially free of three-dimensional (3-D) TiO_x clusters, with isolated bright spots on the terraces and at the step edges. The 11% Ti surface (Figure 2b) is similarly flat with bright areas at the step edges with islands of TiO_x apparent on the terraces. Still more TiO_x islands are formed with an increase in the Ti coverage to 17% as seen in Figure 2c. Surfaces containing >20% Ti show an additional ordered atomic structure on the terraces with atomic

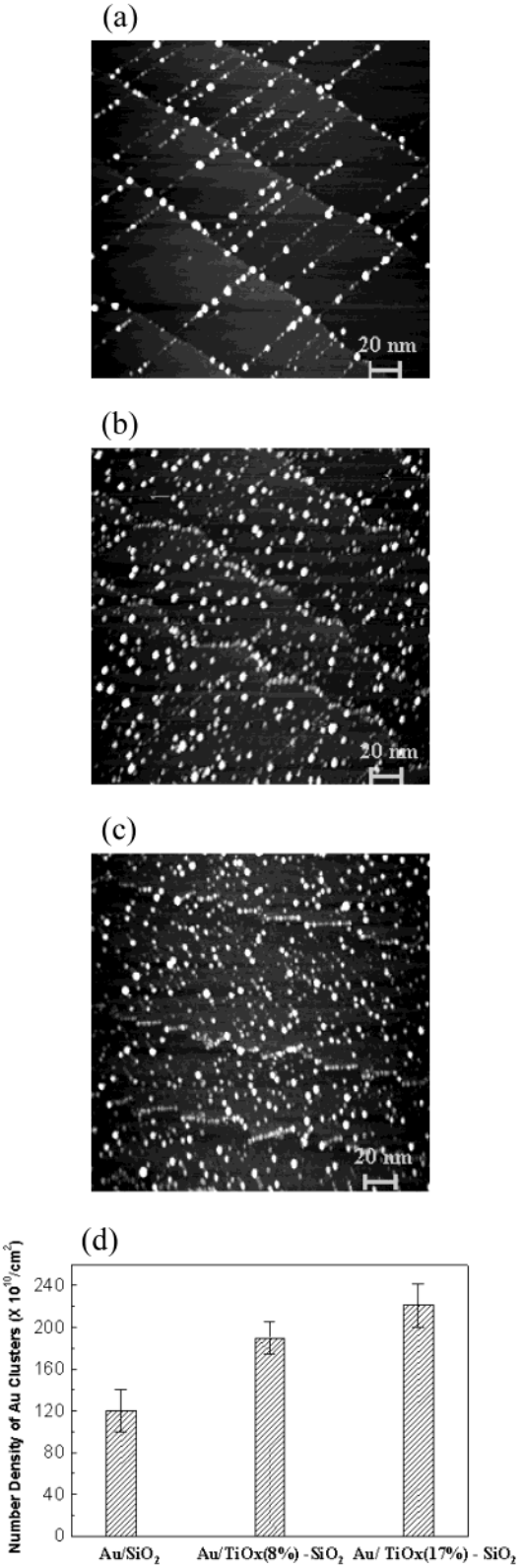

Figure 5. STM images (200 nm × 200 nm, $U_s = -1.7$ V, and $I = 0.18$ nA) of Au nanoclusters on (a) clean SiO_2, (b) $TiO_x(8\%)-SiO_2$, and (c) $TiO_x(17\%)-SiO_2$. The clusters decorate the line defects and step edges of the bare silica film but begin to nucleate on the terraces with increasing Ti coverage. (d) The number density of Au nanoclusters for each state estimated from the corresponding STM images showing an increase in Au cluster density with respect to Ti content.

row distances of ~1.3 nm near the step edges, similar to the missing row structure observed for the Ti_2O_3 reconstructed surface.[24]

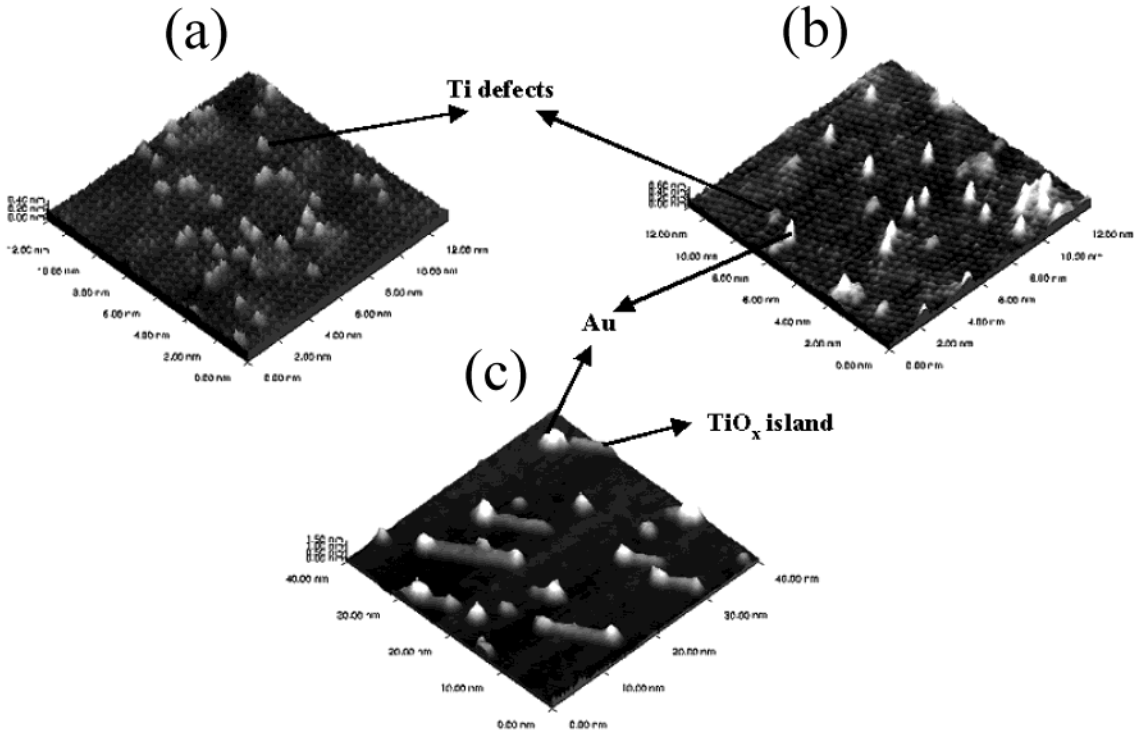

Figure 6. 3-D STM images of (a) $TiO_x(8\%)-SiO_2$, (b) Au(0.04 ML)/$TiO_x(8\%)-SiO_2$, and (c) Au (0.08 ML)/$TiO_x(17\%)-SiO_2$ showing that both Ti defects and TiO_x islands play a role as nucleation sites for Au nanoclusters.

High-resolution STM images of an 8% TiO_x-SiO_2 surface acquired with two extreme bias modes are shown in Figure 3a,b. The images show a collection of bright spots corresponding to Ti atoms and less distinct bright areas corresponding to corrugations of the SiO_2 thin film surface. The brightest areas, corresponding to the Ti atoms, appear along the $[11\bar{1}]$ direction. The height difference (Figure 3c) of these bright spots is approximately 0.1 nm, considerably less than the Ti−O bond length, consistent with the Ti atoms that lie in the plane of the SiO_2 film rather than on the surface. The average number density of these bright spots on the terrace estimated from the STM images is approximately $3.0 \times 10^{13}/cm^2$ with the highest density at or near the step edges as shown in Figure 3d.

The contrast of the Ti atoms is independent of the STM bias as seen in Figure 3a,b; however, differences were observed in the atomic corrugations of the Ti-free SiO_2 surface. The contrast is amplified in the enlarged STM images of Figure 4a,b. The image (Figure 4a) obtained with negative sample bias shows bright spots corresponding to $c(2 \times 2)$ units, consistent with our previous atomically resolved STM images of a clean SiO_2 thin-film surface.[23] However, contrast between the features in the $c(2 \times 2)$ units along the $[11\bar{1}]$ direction is apparent but with essentially no contrast in the $[1\bar{1}0]$ direction. The contrast along the $[11\bar{1}]$ direction becomes much clearer in the STM images (Figure 4b) obtained by reversing the bias. In addition to the primary $c(2 \times 2)$ units, additional spots with sharp contrast and less apparent atomic corrugation appear in the $c(2 \times 2)$ units along the $[11\bar{1}]$ direction. These images are consistent with the existence of two species with differing geometries aligned in essentially the same direction, since this surface shows a $c(2 \times 2)$ LEED pattern (Figure 1b) and all atomic features are aligned along the $[11\bar{1}]$ direction. Therefore, the small difference leading to a $c(2 \times 2)$ structure and alternation of smaller and larger atomic corrugations in the STM images could result from a small height difference due to the Si−O−Si network.

Figure 4c is a high-resolution STM image of the local terrace area of the TiO_x-SiO_2 surface. The brightest spots along the $[11\bar{1}]$ direction correspond approximately to the size of two atomic corrugations of the SiO_2 surface. Upon annealing to 1150 K, a slight decrease in the Si/Mo Auger intensity ratio was observed. Since a pure SiO_2 thin film is stable at 1150 K, the Si loss is assumed to be induced by the Ti. Furthermore, the LEED data shows no change from a very sharp $c(2 \times 2)$ diffraction pattern, implying that these bright spots do not inhibit the long-range order of the film. The Si atoms in the SiO_2 matrix then are apparently replaced with Ti atoms, where the Ti atoms form a local tetrahedral network within the SiO_2 matrix similar to that found in TiO_2-SiO_2 mixed oxides dilute in Ti. The sharp contrast of the substituted Ti atoms in the STM images can relate to geometric and/or electronic effects; however, geometric effects are likely dominant since no significant change is observed upon reversal of the imaging bias (Figure 3a,b). The average Ti−O bond length is 0.180−0.196 nm depending upon coordination,[13] considerably larger than the Si−O bond length of 0.161 nm in SiO_2.

The bright spot doublets (bright spot triplets are also observed, but these constitute less than 2%) are consistent with one Ti atom influencing two neighboring oxygen atoms if the bright spots are assumed to be oxygen atoms. The total Ti content on the terraces of the SiO_2 thin film calculated from the STM images is approximately $3.6 \pm 0.4\%$ of the SiO_2 surface, less than the Ti coverage. However, as seen in the STM image of Figure 3d, the brightest spots are much more dense at or near the step edges of the SiO_2 thin film, with a corresponding lower than average concentration on the terraces. This surface, then, consists of an atomically mixed TiO_2-SiO_2 planar surface with atomically substituted Ti defects.

Defects on oxide surfaces play a key role in the nucleation and growth of metal nanoclusters.[7,28,29] Recently, Besenbacher and co-workers showed that bridging oxygen vacancies on TiO_2 serve as nucleation sites for Au clusters.[7] In addition, based on the STM observations of Besenbacher and co-workers, the diffusion of cluster-vacancies plays an important role in the formation of larger Au clusters. In related work, Freund and

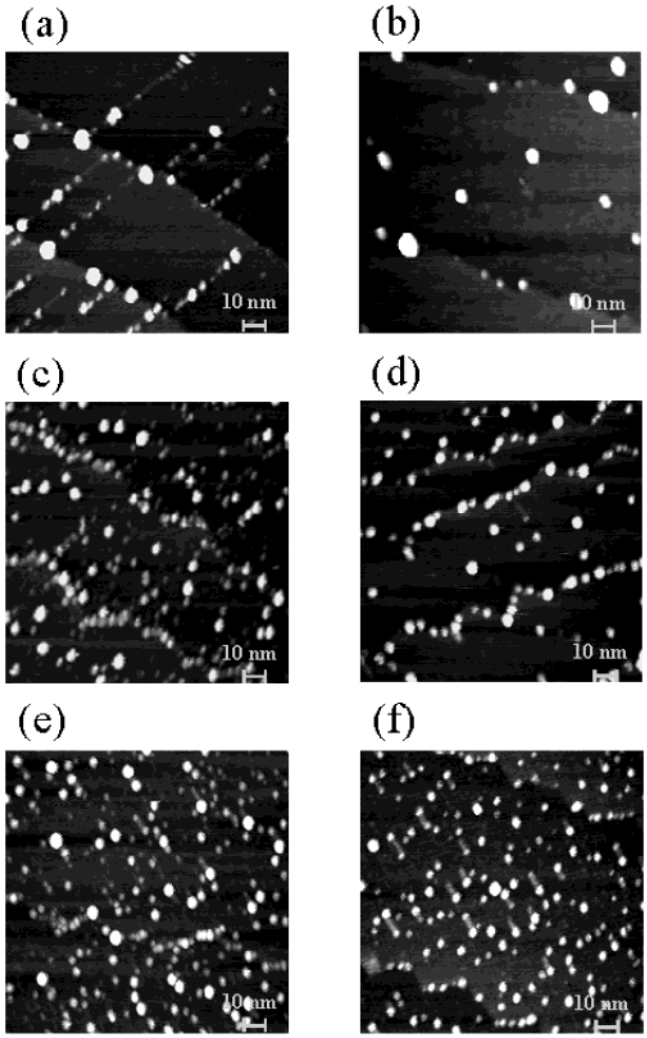

Figure 7. STM images (100 nm × 100 nm, $U_s = -1.7$ V, and $I = 0.18$ nA) of Au (0.4 ML) clusters: (a) nucleated on a Ti-free SiO_2 thin at room temperature; (b) clusters of a annealed to 850 K; (c) nucleated on a $TiO_x(8\%)-SiO_2$ thin film at room temperature; (d) clusters of c annealed to 850 K; (e) nucleated on a $TiO_x(17\%)-SiO_2$ thin film at room temperature; and (f) clusters of e annealed to 850 K.

co-workers reported decoration of line defects by Pd and Rh clusters on an Al_2O_3 surface.[30]

Three kinds of defects are anticipated in our SiO_2 thin films: extended defects (e.g., steps and kinks), line defects (e.g., antiphase domain boundaries), and point defects (e.g., oxygen vacancies). Au clusters preferentially nucleate and grow along line defects at room temperature, as evident in the STM images of Figure 5a. Line defects in SiO_2 thin films have been proposed by Freund and co-workers, based on the broadened superlattice spots in LEED, to arise from antiphase domain boundaries.[17]

Enhancement of the cluster density is readily apparent when the same amount of Au (0.4 ML) is deposited on clean and Ti-modified SiO_2 surfaces. For the Ti-free, 8% TiO_2-SiO_2, and 17% TiO_2-SiO_2 surfaces (parts a, b, and c of Figure 5, respectively), Au cluster decoration is dramatically different, consistent with the Ti defects described above serving as nucleation and growth sites. The histogram of Figure 5d illustrates the relationship between Ti coverage and Au cluster density.

The STM image in Figure 6a shows an 8% Ti-covered SiO_2 surface on which the Ti defects are evident as bright areas. Figure 6b shows the same surface after deposition of 0.04 ML

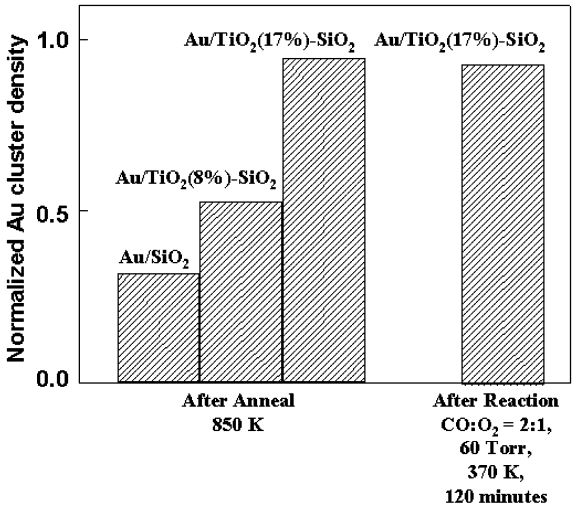

Figure 8. Histogram of Au cluster density after the indicated treatment normalized to the cluster density after nucleation at room temperature. The Au coverage in each of the experiments was 0.4 ML Au. The first three columns compare the cluster density on Ti-free SiO_2, $TiO_x(8\%)-SiO_2$, and $TiO_x(17\%)-SiO_2$ thin films, respectively, after a 850 K anneal. The fourth column shows the normalized Au cluster density of a $TiO_x(17\%)-SiO_2$ thin film after a CO oxidation reaction ($CO:O_2 = 2:1$, 60 Torr, 370 K, and 120 min).

Au, where the deposited clusters exhibit additional brightness over and above that of the Ti defects. The height difference between the spots corresponding to the Ti defects and those corresponding to the Au clusters is approximately 0.2 nm. Figure 6c shows a 17% Ti-covered surface after deposition of 0.08 ML Au, where the metal clusters clearly decorate primarily the extremities of TiO_x islands. It is noteworthy that the number density of Au clusters at 0.4 ML Au coverage is approximately 1 order of magnitude lower than the number density of Ti defects, consistent with cluster-promoted agglomeration of Ti defects.[7]

The number density of Au clusters decreases upon further addition of Ti. For the >20% Ti-modified SiO_2 surface, an ordered TiO_x surface forms first at the step edges and then on the terraces. This ordered TiO_x surface shows an atomic row structure where the distance between the rows is approximately 1.3 nm, close to the $p(n \times 3)$ Mo(112) structure and the missing row structure of Ti_2O_3.[24] This ordered surface is much less efficient for Au cluster nucleation.

Because there is a relatively weak interaction between SiO_2 and noble metals,[31] thermal sintering is observed for SiO_2-supported noble-metal clusters. For example, Au clusters nucleated on a SiO_2 thin film (Figure 7a) sinter when heated to 850 K, resulting in a dramatic decrease in the cluster density and an increase in cluster size (Figure 7b). Sintering is also observed for Au clusters on TiO_2-SiO_2 surfaces with relatively low coverages of Ti, e.g., 8%, as is evident in Figure 7c before and in Figure 7d after an 850 K anneal. However, sinter-resistant properties are observed when the Ti coverage is increased to 17% (Figure 7e), showing no apparent morphological change after heating to 850 K (Figure 7f). The histogram of Figure 8 shows the Au cluster density after an 850 K anneal and after reaction in $CO + O_2$ relative to the cluster density following nucleation at room temperature for the Ti-free, 8% TiO_2-SiO_2, and 17% TiO_2-SiO_2 surfaces, respectively. An approximately 70% decrease in Au cluster density is observed on the Ti-free surface due to the thermally induced sintering effect, whereas the extent of sintering of Au clusters is attenuated significantly with an increase in the Ti coverage, with no apparent sintering

for the 17% Ti-covered SiO_2 surface. The sinter-resistant properties of the 17% Ti-covered SiO_2 surface were further tested by exposing the sample to CO oxidation reaction conditions ($CO:O_2 = 2:1$, 60 Torr, ~370 K, and 120 min). The cluster density following reaction (Figure 8) shows no significant decrease. Therefore, it is apparent that the mixed-oxide surface exhibits sinter-resistant properties with respect to thermal treatment and high-pressure gas exposure.

The origin of the observed sinter-resistant properties for the titania−silica mixed-oxide surface is unclear and currently under investigation. However, the formation of 2-D and/or 3-D TiO_x islands is likely important, possibly in physically confining the Au clusters, since silica surfaces with only atomically substituted Ti do not show significantly altered sintering properties.

Conclusions

These STM studies demonstrate that a titania−silica mixed-oxide surface containing atomically substituted Ti defects can be synthesized. These atomic Ti defects are formed by substitution of Si atoms with Ti atoms in a SiO_2 matrix where Ti atoms form a local tetrahedral network. In addition, these defects induce a significant increase in the number density of Au clusters by serving as nucleation sites. A titania−silica surface with TiO_x islands was also synthesized at Ti coverages greater than 10%. Both atomically substituted Ti defects and TiO_x islands serve as nucleation and growth sites for Au nanoclusters. Au nanoclusters supported on a mixed-oxide surface containing TiO_x islands, formed by the addition of 17% Ti, show no apparent change in density and size, implying sinter-resistant properties for Au nanoclusters toward thermal treatment and high-pressure gas exposure.

Acknowledgment. We acknowledge with pleasure the support of this work by the U.S Department of Energy, Office of Basic Energy Science, Division of Chemical Sciences, U.S. Civilian Research & Development Foundation, and the Texas Advanced Technology Program under Grant no. 010366-0022-2001.

References and Notes

(1) Haruta, M. *Catal. Today* **1997**, *36*, 153.
(2) Valden, M.; Lai, X.; Goodman, D. W. *Science* **1998**, *281*, 1647.
(3) Hayashi, T.; Jan, L. B.; Tsubota, S.; Haruta, M. *Ind. Eng. Chem. Res*. **1995**, *34*, 2298.
(4) Mul, G.; Zwijnenburg, A.; Linden, B.; Makkee, M.; Moulijn, J. A. *J. Catal*. **2001**, *201*, 128.
(5) Stangland, E. E.; Stavens, K. B.; Andres, R. P.; Delgass, W. N. *J. Catal*. **2000**, *191*, 332.
(6) Sanchez, A.; Abbet, S.; Heiz, U.; Schneider, W.-D.; Hakkinen, H.; Barnett, R. N.; Landman, U. *J. Phys. Chem. A* **1999**, *103*, 9573.
(7) Wahlstrom, E.; Lopez, N.; Schaub, R.; Thostrup, P.; Ronnau, A.; Africh, C.; Lægsgaard, E.; Nørskov, J. K.; Besenbacher, F. *Phys. Rev. Lett*. **2003**, *90*, 026101−1.
(8) Lopez, N.; Nørskov, J. K. *Surf. Sci*. **2002**, *515*, 175.
(9) Haruta, M. *Chem. Rec*. **2003**, *3*, 75.
(10) Valden, M.; Pak, S.; Lai, X.; Goodman, D. W. *Catal. Lett*. **1998**, *56*, 7.
(11) Wynblatt, P.; Gjostein, N. A. *Acta Metall*. **1976**, *24*, 1165.
(12) Lai, X.; St Clair, T. P.; Goodman, D. W. *Faraday Discuss*. **1999**, *114*, 279.
(13) Gao, X.; Wachs, I. E. *Catal. Today* **1999**, *51*, 233 and references therein.
(14) Nijhuis, T. A.; Huizinga, B. J.; Makkee, M.; Moulijn, J. A. *Ind. Eng. Chem. Res*. **1999**, *38*, 884.
(15) Clark, H. W.; Bowman, R. G.; Maj, J. J.; Bare, S. B.; Hartwell, G. E. U.S. Patent 5,965,754, 1999.
(16) Lai, X.; St Clair, T. P.; Goodman, D. W. *Prog. Surf. Sci*. **1998**, *59*, 25.
(17) Schroeder, T.; Giorgi, J. B.; Bäumer, M.; Freund, H.-J. *Phys. Rev. B* **2002**, *66*, 165422.
(18) Schroeder, T.; Giorgi, J. B.; Bäumer, M.; Freund, H.-J. *Surf. Sci*. **2002**, *498*, L71.
(19) Min, B. K.; Santra, A. K.; Goodman, D. W. *Catal. Today* **2003**, *85*, 113.
(20) Schroeder, T.; Giorgi, J. B.; Hammoudeh, A.; Magg, N.; Bäumer, M.; Freund, H.-J. *Phys. Rev. B* **2002**, *65*, 15411.
(21) Tanuma, S.; Powell, C. J.; Penn, D. R. *Interface Anal*. **1991**, *17*, 911.
(22) Wendt, S.; Kim, Y. D.; Goodman, D. W. *Prog. Surf. Sci*. **2003**, *74*, 141.
(23) Ozensoy, E.; Min, B. K.; Santra, A. K.; Goodman, D. W. *J. Phys. Chem. B* **2004**, *108*, 4351.
(24) Sander, M.; Engel, T. *Surf. Sci. Lett*. **1994**, *302*, L263.
(25) Eitel, W. *The Physical Chemistry of the Silicates;* University of Chicago Press: Chicago, IL, 1954.
(26) Wagner, C. D.; Naumkin, A. V.; Kraut-Vass, A.; Allison, J. W.; Powell, C. J.; Rumble, J. R., Jr. *NIST Standard Reference Database 20*, version 3.4; web version.
(27) Black, L.; Garbev, K.; Stemmermann, P.; Hallam, K. R.; Allen, G. C. *Cem. Concr. Res*. **2003**, *33*, 899.
(28) Haas, G.; Menck, A.; Brune, H.; Barth, J. V. *Phys. Rev. B* **2002**, *61*, 11105.
(29) Bogicevic, A.; Jennison, D. R. *Surf. Sci*. **2002**, *515*, L481.
(30) Bäumer, M.; Frank, M.; Heemeier, M.; Kuhnemuth, R.; Stempel, S.; Freund, H.-J. *Surf. Sci*. **2000**, *454*, 957.
(31) Tauster, S. J.; Fung, S. C.; Baker, R. T. K.; Horsley, J. A. *Science* **1981**, *211*, 1121.